A Comprehensive Study of Formic Acid Oxidation on Palladium Nanocrystals with Different Types of Facets and Twin Defects

Sang-Il Choi, [a] Jeffrey A. Herron, [b] Jessica Scaranto, [b] Hongwen Huang, [a] Yi Wang, [a] Xiaohu Xia, [a] Tian Lv, [a] Jinho Park, [a] Hsin-Chieh Peng, [a] Manos Mavrikakis, [b] and Younan Xia*[a]

- [a] Dr. S.-I. Choi, H. Huang, Y. Wang, Dr. X. Xia, T. Lv, J. Park, H.-C. Peng, Prof. Y. Xia
 The Wallace H. Coulter Department of Biomedical Engineering, School of Chemistry and
 Biochemistry, and School of Chemical and Biomolecular Engineering
 Georgia Institute of Technology, Atlanta, Georgia 30332 (USA)
 E-mail: younan.xia@bme.gatech.edu
- [b] Dr. J. A. Herron, Dr. J. Scaranto, Prof. M. Mavrikakis
 Department of Chemical and Biological Engineering
 University of Wisconsin-Madison, Madison, Wisconsin 53706 (USA)

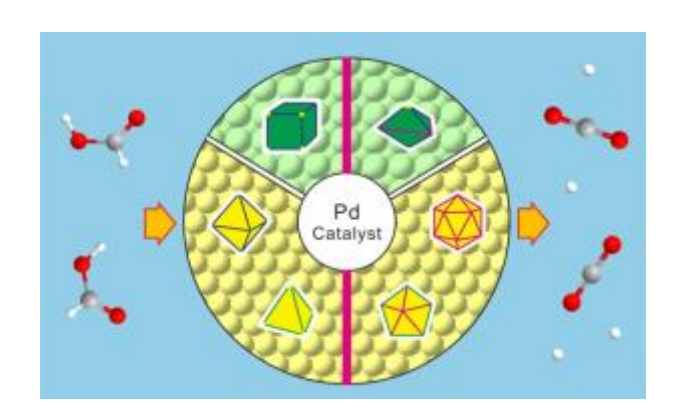
Supporting information for this article is available on the WWW under http://dx.doi.org/.

Abstract

Palladium has been recognized as the best anodic, monometallic electro-catalyst for the formic acid oxidation (FAO) reaction in a direct formic acid fuel cell. Here we report a systematic study of FAO on a variety of Pd nanocrystals, including cubes, right bipyramids, octahedra, tetrahedra, decahedra, and icosahedra. These nanocrystals were synthesized with roughly the same size, but different types of facets and twin defects on their surfaces. Our measurements indicate that the Pd nanocrystals enclosed by {100} facets have higher specific activities than those enclosed by {111} facets, in agreement with prior observations for Pd single-crystal substrates. When comparing nanocrystals predominantly enclosed by a specific type of facet, {100} or {111}, those with twin defects showed greatly enhanced FAO activities compared to their single-crystal counterparts. To rationalize these experimental results, we performed periodic, self-consistent density functional theory calculations on model single-crystal substrates of Pd, representing the active sites present in the nanocrystals used in the experiments. The calculation results suggest that the enhancement of FAO activity on defect regions, represented by Pd(211) sites, when compared to the activity of both Pd(100) and Pd(111) surfaces, could be attributed to an increased flux through the HCOO-mediated pathway rather than the COOH-mediated pathway on Pd(211). Since COOH has been identified as a precursor to CO, a site-poisoning species, a lower coverage of CO at the defect regions will lead to a higher activity for the corresponding nanocrystal catalysts, containing those defect regions.

Keywords: Pd nanocrystals · formic acid oxidation · shape-controlled synthesis · twin defect

Pd catalysts for formic acid oxidation: This work systematically evaluated the activities of Pd nanocrystals with different types of facets and twin defects towards formic acid oxidation.



Introduction

Direct liquid fuel cells involving electrochemical oxidation of liquid fuels on the anodes have received considerable interest as the next-generation power sources for portable devices such as smart phones and laptops. [1-3] For several decades, methanol has been widely explored as a liquid fuel for such devices due to its high energy density. However, methanol is toxic and its electro-oxidation is plagued by problems such as production of CO, and thus poisoning of the catalyst, as well as crossover flux through the membrane. Ethanol, another promising liquid fuel, also generates CO during its electro-oxidation. Most of these issues can be addressed by switching to a liquid fuel based on formic acid. For example, the level of CO produced from formic acid oxidation (FAO) could be lower than that from the oxidation of methanol or ethanol by applying Pd catalyst, which will be discussed in later paragraphs. [4-6] It is also feasible to use formic acid at a higher concentration than methanol because of its reduced toxicity and crossover flux. As a result, FAO on various types of electro-catalysts has received considerable attention in recent years for fuel cell applications.

It has been established that FAO can proceed through two different pathways.^[4,7] In the direct oxidation pathway, CO₂ is formed after two steps of proton/electron transfer, and CO₂ can readily desorb from the surface of a catalyst due to weak binding, liberating active sites for further catalytic reactions. In the indirect oxidation pathway, CO is formed after CO-O bond scission in a carboxyl (COOH) intermediate. CO binds strongly to the surface of a catalyst and acts as a poison, which must be oxidized to CO₂ in the following step in order to be removed from the catalyst. The direct pathway is dominant at low potentials around 0.4 V (vs. reversible hydrogen electrode, RHE) while the indirect pathway occurs at potentials over 0.8 V.^[8] Typically, it is more efficient to oxidize formic acid through the direct pathway, but the gradual accumulation of CO at potentials around 0.4 V may still diminish the catalytic activity after many cycles of reaction. An ideal catalyst for FAO should work at potentials around 0.4 V, together with an ability to prevent the formation of CO and/or resist the poisoning by CO.

Palladium is considered the most effective catalyst for FAO owing to its high activity in directly oxidizing formic acid to CO₂ at relatively low potentials.^[7] The high activity can be attributed to the low CO formation flux, thereby mitigating the poisoning effect of CO as compared with Pt, another catalyst that has been explored for FAO.^[9,10] Although the Pd catalyst can still be deactivated because of the gradual accumulation of CO during operation, the high activity can be replenished by increasing the potential beyond 1.0 V.^[11] The activity of a Pd catalyst is typically determined by the arrangement of atoms on the surface. For the

low-index facets on Pd single-crystal substrates, their FAO activities increase in the order of Pd(110) < Pd(111) < Pd(100). [10] Over the past decade, there has been a strong interest in controlling the shape of Pd nanocrystals to preferentially expose the most active {100} facets. In a previous study, we tested Pd cubes and octahedra as two model systems to understand the dependence of FAO activity on crystal facet.^[14] In good agreement with the results obtained from single-crystal substrates, Pd cubes enclosed by {100} facets were found to be more active than octahedra enclosed by {111} facets. In addition to the type of facet, the twin defect or stacking fault on the surface of a Pd nanocrystal can also affect its performance in catalyzing FAO.^[16-24] Recently, we demonstrated that the specific activity (j/mA cm⁻²) toward FAO on Pd icosahedra was two-fold higher than that of Pd octahedra, even though both geometries are predominantly exposing (111) facets.^[16] This enhancement could be attributed to the presence of twin defects on the surface of Pd icosahedra. We also studied the effect of twin defects on the FAO activity by comparing Pd right bipyramids with single-crystal Pd cubes, and a two-fold enhancement was observed.[17] The enhancement in activity could be attributed to the {211} facets exposed on the twin defect of a Pd right bipyramid. The reaction on this high-index facet prefers the HCOO-mediated pathway, helping reduce the formation of CO.

Herein, we report, for the first time, a comprehensive and systematic study of FAO on Pd nanocrystals with different types of facets and twin defects, including cubes, right bipyramids, octahedra, tetrahedra, decahedra, and icosahedra (Scheme 1). To minimize the effect of size, [25] all the Pd nanocrystals were prepared with a similar size in the range of 13-17 nm for edge lengths or diameters (Table 1). Their corresponding FAO activities were then measured using the same setup and under essentially identical conditions to minimize any possible variations or errors.^[7,10,12-18] Both the cubes and right bipyramids are enclosed by {100} facets, while the octahedra, tetrahedra, decahedra, and icosahedra are all enclosed by {111} facets. The Pd nanocrystals enclosed by {100} facets showed higher specific activity than those enclosed by {111} facets, in agreement with previous observations on Pd single-crystal substrates.^[10] For Pd nanocrystals enclosed by the same type of facet but possessing a singlecrystal or twin structure, those with twin defects on the surfaces showed higher specific activities. At 0.4 V, a potential responsible for the direct oxidation pathway, both the Pd decahedra and icosahedra showed greater specific activities than the octahedra and tetrahedra. In addition, the FAO activity was found to be affected more significantly by the twin defects relative to the difference in low-index facets. In this respect, the decahedra and icosahedra showed higher specific activities than the cubes even they were enclosed by {111} facets

with a lower activity than the {100} facets on cubes. Among all the nanocrystals we have tested, the right bipyramids showed the highest specific activity at 0.4 V. To understand the experimental results, we performed periodic self-consistent density functional theory calculations (DFT, GGA-PW91) on model single-crystal substrates of Pd. Because of the enhancement in flux through the HCOO-mediated pathway on Pd(211) surface, representing the structure of defect sites on the nanocrystals, [24] the level of CO is reduced relative to that on Pd(100) and Pd(111), leaving more catalytic sites on the nanocrystals for the electro-oxidation of formic acid to CO₂.

Results and Discussion

Synthesis of Pd nanocrystals with different types of facets and twin defects

The synthesis of Pd cubes was carried out in the presence of KBr due to the important role of Br ions in promoting the formation of {100} facets.^[14,26] Figure 1A shows a transmission electron microscopy (TEM) image of the as-obtained Pd cubes with an average edge length of 15 nm to demonstrate good uniformity in shape and narrow distribution in size. Figure 1B shows a TEM image of Pd right bipyramids synthesized in the presence of NaI, where I ions can act as an oxidative etchant for the selective removal of multiple-twinned Pd nanoparticles and as a selective capping agent for the {100} facets. [17] The Pd nanocrystals with other shapes such as octahedra and tetrahedra (Figure 1, C and D) were prepared via seed-mediated growth with the use of different combinations of seeds and precursors, including Na₂PdCl₄ and Pd(acac)2. [15] Specifically, 5-nm Pd cuboctahedra were used as seeds for the syntheses of Pd octahedra and tetrahedra with average edge lengths of 13 and 15 nm, respectively, in a mixture of ethylene glycol (EG) and tetraethylene glycol (TTEG). The Pd decahedra (Figure 1E) were prepared with an average diameter of 15 nm by adding Na₂PdCl₄ into a diethylene glycol (DEG) solution containing poly(vinyl pyrrolidone) (PVP) and Na₂SO₄.^[19] The Pd icosahedra were synthesized by adding HCl into the polyol synthesis, which could control the pH value of the solution and thus manipulate the reaction kinetics.^[16] The use of HCl at an optimal concentration could lead to the formation of Pd icosahedra with high purity (>94%) and uniformity. The sample shown in Figure 1F had an average diameter of 17 nm. All the detailed descriptions for the synthesis of Pd nanocrystals with different shapes are presented in the Experimental Section.

Figure 2 shows simple geometric models of two different types of twin defects that are involved in the Pd nanocrystals evaluated by this work. The first type of twin defect is a mirror symmetry plane that can be introduced into the lattice of a crystal without causing any strain to the lattice. A typical example is the right bipyramid, which is bisected by a symmetry plane along the <111> direction in the middle of the nanocrystal and enclosed by six right-isosceles triangular {100} facets, as shown in Figure 2A. This type of twin defect only leads to the formation of three {211} high-index facets on the nanocrystal, and it does not cause strains to the crystal lattice.^[17]

The other type of twin defect corresponds to the boundary region between two tetrahedral units in a decahedron or icosahedron. As shown in Figure 2B, a decahedral nanocrystal can be considered to form from five tetrahedral units (all covered by {111} facets) by sharing one common edge along the five-fold axis. A total of five twin boundaries are required to generate the decahedral particle because it is impossible to completely fill the space of a particle in five-fold symmetry with a single-crystal lattice only. Specifically, the projection angle of 70.53° for each tetrahedral unit brings a gap of 7.35° when the five tetrahedral units are assembled together by sharing one common edge, leading to the formation of strained regions at the boundaries. Johnson and coworkers recently demonstrated that the twin boundary of a decahedron is characterized by disclination and graded strains in the crystal lattice.^[21] From the rigid-body rotation measurement, they found that a gap of 4.3° could be filled through atomic disclination while the remaining gap had to be filled through graded shear strains on the lattice.^[21] An icosahedron consists of twenty tetrahedral units with thirty twin boundaries and twenty {111} facets. [16,22-24] As shown in Figure 2C, the twin defect of a Pd icosahedron corresponds to a gap of 1.54 steradians. [27] Since every edge on an icosahedron is a result of twin boundaries, the density of twin boundaries on the surface of an icosahedron is higher than that on the decahedron. The facets corresponding to the twin boundaries of a decahedron can be indexed as $\{211\}$ based on its projection along the $[0\overline{1}1]$ zone axis, as shown in Figure S1. Because an icosahedron is comprised of twelve interpenetrating decahedra, the twin boundaries of an icosahedron can also be assigned to the {211} facets.

Electrochemical measurements of the Pd nanocrystals

The surfaces of the as-synthesized Pd nanocrystals were covered by capping agents such as Br-, I-, and PVP. Therefore, we performed plasma etching for 30 min, followed by holding the electrical potential at -0.05 V (vs. RHE) for 60 s to remove the capping agents prior to

electrochemical measurements.^[7,17] To minimize the effect of particle size on FAO, ^[25] all the Pd nanocrystals were prepared with edge lengths or diameters in the range of 13-17 nm (Figure 1). Figure S2 shows typical cyclic voltammograms (CVs) between 0.08 and 0.8 V for the Pd nanocrystals obtained in N2-saturated solutions containing 0.1 M HClO4. From the curves, we could easily identify the hydrogen adsorption/desorption peaks. To evaluate the electrocatalytic surface areas (ECSAs), we performed stripping of underpotentially deposited Cu (Cuupd) prepared in a N2-saturated solution containing 0.05 M H2SO4 and 0.05 M CuSO4. As shown by the Cuupd curves in Figure S3, the Pd nanocrystals exhibited different behaviors. For the nanocrystals enclosed by {100} facets, a single Cuupd peak appeared at 0.56 V for cubes and at 0.57 V for RBPs, respectively (Figure S3A). ^[28] The Cuupd peaks for the Pd nanocrystals enclosed by {111} facets all appeared below 0.53 V (Figure S3B). ^[28] The ECSAs of the catalysts were calculated by integrating the stripping charges of Cuupd. Charges of 420 and 490 μ C cm⁻² were used for the Pd{100} and Pd{111} facets, respectively. ^[7,16,17]

We then conducted electrochemical measurements of FAO for the Pd nanocrystals with different shapes using the same setup and under essentially identical conditions (see details in the Experimental Section) to minimize any possible variations or errors. [7,10,12-18] We first compared the electro-catalytic activities between the nanocrystals enclosed by {100} and {111} facets, and then compared those with a single-crystal or twinned structure. Figure 3 shows the CVs of FAO for the catalysts recorded between 0.08 and 1.1 V in N2-saturated solutions containing 0.5 M HClO₄ and 0.5 M HCOOH at a scan rate of 50 mV s⁻¹. The specific activity was obtained by normalizing to the ECSA of the catalyst derived from the charges of Cuupp. The anodic CVs of FAO for Pd nanocrystals enclosed by {100} facets, such as cubes and right bipyramids, are shown in Figure 3A. At the anodic peak potential, the specific activity of the right bipyramids was much higher than that of the cubes (Table 1). Figure 3B shows the anodic CVs of FAO for Pd nanocrystals enclosed by {111} facets, including octahedra, tetrahedra, decahedra, and icosahedra. For both the decahedra and icosahedra with twinned structures, they showed enhancement in specific activity at the anodic peak potential relative to the single-crystal octahedra and tetrahedra (Table 1). To better quantitatively compare the catalytic activities of these Pd nanocrystals, their specific activities at 0.4 V, a potential for the direct oxidation pathway, [7] are summarized in Figure 4 and Table 1. The cubes enclosed by {100} facets showed enhancement in specific activity relative to both the octahedra and tetrahedra enclosed by {111} facets, in agreement with the results of previous studies for single-crystal substrates.^[10] The nanocrystals with twin defects

(*i.e.*, right bipyramids, decahedra, and icosahedra) demonstrated enhanced specific activity with respect to their single-crystal counterparts (*i.e.*, right bipyramids were more active than cubes while the decahedra or icosahedra were more active than octahedra or tetrahedra). Between decahedra and icosahedra, the latter sample exhibited slightly higher activity than the former one. This result could be explained by the larger number of twin boundary regions on the surface of an icosahedron than that on a decahedron (Table 1). In addition, both decahedra and icosahedra showed enhanced specific activity at 0.4 V relative to the cubes even they were enclosed by {111} facets that are less active than {100}. Taken together, it can be concluded that the FAO activity could be enhanced more significantly by including twin defects rather than by varying the low-index facets from {111} to {100}.

DFT calculations for FAO on Pd nanocrystals

To rationalize the experimental observations, we performed periodic self-consistent DFT calculations (GGA-PW91) on model single-crystal surfaces, which would capture the various types of active sites that may be present in the nanocrystals our experiments were performed on. The twin defect on the surface of a right bipyramid, decahedron, or icosahedron was modeled as a Pd(211) surface (Figure S1). The terraces in the defect zone were modeled as Pd(111) and Pd(100) surfaces. We evaluated the potential energy surfaces at 0.4 V for FAO through two reaction pathways (see Figure 5, the binding energies used to construct the potential energy surface are provided in Table S1): carboxyl-mediated and formate-mediated. As shown in Table 2, the carboxyl (COOH) species, which has been identified as a precursor to CO formation, is more stable than formate (HCOO) by 0.22 eV on Pd(100) and more stable by 0.11 eV on Pd(111). In contrast, HCOO and COOH are iso-energetic on Pd(211). The relative stability of HCOO over COOH drives the reaction flux and selectivity toward the HCOO-mediated pathway rather than the COOH-mediated pathway. This result is important because, on all these surfaces, it is thermochemically favorable for COOH to be dissociated into CO and OH. If formed, the CO will compete with HCOO for the surface sites, poisoning the surface and lowering its catalytic activity. We note that in our calculations, the potential energy of surface did not include the stabilization effect of water toward adsorbed OH, which has been calculated to be $\sim 0.5 \ eV$ on Pt(111), [29] which, in turn, would make CO oxidation by OH to CO₂ more difficult than it appears in Figure 5. Therefore, by enhancing flux through the HCOO-mediated pathway on Pd(211), the formation of CO will be reduced relative to those on Pd(100) and Pd(111), leaving relatively more catalytic sites on Pd(211) free of CO (compared to (100) and (111)) for FAO to directly produce CO₂.

We also investigated the role of surface strain (up to $\pm 5\%$) on the binding properties of Pd(211) surfaces to examine the impact of dislocation and shear gradients resulting from the twin defects on decahedra and icosahedra. There were only very small changes to the binding characteristics (see details in the supporting information, as well as Table S2 and Figure S4). Additionally, the effect of strain on the relative stability of HCOO vs. COOH intermediates was probed on Pd(111) with 0-3% tensile strain (see details in the supporting information and Table S3),[30] and the effect was again found to be minimal, almost negligible when compared to the magnitude of change between different types of facets. Overall, this simple analysis provides one possible explanation for the observed enhancement in activity on the nanocrystals with twin defects when compared to their single-crystal counterparts. A more detailed mechanistic analysis may be required to evaluate other possible mechanisms responsible for the observed activity enhancement.

Conclusion

In summary, we have systematically investigated the FAO activities of Pd nanocrystals with different shapes and twin structures, including cubes, right bipyramids, octahedra, tetrahedra, decahedra, and icosahedra. The nanocrystals enclosed by {100} facets were found to show higher specific activities than those enclosed by {111} facets. For nanocrystals enclosed by the same type of facet but with a single-crystal or twin structure, those with twin defects on the surfaces showed higher specific activities. It is interesting to note that both decahedra and icosahedra exhibited higher specific activities than cubes even though the {111} facets are less active than the {100} facets. In these cases, the presence of twin defects imposes a stronger impact on the catalytic activity toward FAO than the type of facet. To understand the correlation between the specific activity and the twin defect on the nanocrystal, DFT calculations were performed on model single-crystal surfaces of Pd. The formation of CO is reduced on Pd(211) when compared to both Pd(100) and Pd(111), retaining a higher fraction of the defect sites free of CO, for FAO.

Experimental Section

Chemicals and materials

Palladium(II) chloride (PdCl₂, 99.9 %), Na₂PdCl₄ (99.99%), Pd(acac)₂ (99.0%), PVP (MW ≈ 55,000), L-ascorbic acid (AA, 99.0%), KBr (99.0%), NaI (99.5%), Na₂SO₄ (99.0%), DEG (99.0%), TTEG (90%), and HCl (37%) were all purchased from Sigma-Aldrich and used as

received without further purification. EG (99.0%) was obtained from J. T. Baker. Deionized (DI) water with a resistivity of 18.2 M Ω cm was used for all experiments.

Syntheses of Pd cubes and right bipyramids

For the synthesis of Pd cubes with an edge length of 15 nm,^[14] 8.0 mL of an aqueous solution containing PVP (105 mg), AA (60 mg), and KBr (500 mg) was placed in a 20 mL vial. The mixture was pre-heated at 80 °C for 10 min under magnetic stirring. Then, 3.0 mL of an aqueous solution containing Na₂PdCl₄ (57 mg) was rapidly injected into the vial using a pipette. The reaction solution was allowed to proceed at 80 °C for 3 h.

For the synthesis of Pd right bipyramids with an edge length of 15 nm along the <100> direction, [17] 5.0 mL of EG containing PVP (400 mg) and NaI (150 mg) was added into a 25 mL three-neck, round-bottom flask. The mixture was pre-heated at 160 °C for 10 min under magnetic stirring. Then, 1.0 mL of EG containing Na₂PdCl₄ (15 mg) was rapidly injected into the flask with a pipette. The reaction solution was allowed to proceed at 160 °C for 2 h.

Syntheses of Pd octahedra, tetrahedra, decahedra, and icosahedra

For the syntheses of Pd octahedra and tetrahedra (with edge lengths of 13 and 15 nm, respectively), [15] 2.5 mL of TTEG containing PVP (10 mg) and 0.1 mL of a suspension of the 5-nm cuboctahedral Pd seeds in EG (1.8 mg mL⁻¹ in concentration) were placed in a 20 mL vial. The mixture was pre-heated at 140 °C for 10 min under magnetic stirring. Meanwhile, 0.5 mL of TTEG solution containing Na₂PdCl₄ (2 mg) or an equal molar amount of Pd(acac)₂ was prepared for the synthesis of Pd octahedra or tetrahedra, respectively. After the precursor had been completely dissolved, the solution was quickly injected into the vial using a pipette. The reaction solution was allowed to proceed at 140 °C for 1 h.

For the synthesis of Pd decahedra 15 nm in diameter,^[19] 2.0 mL of DEG containing PVP (80.0 mg) and Na₂SO₄ (40.0 mg) was placed in a 20 mL vial. The mixture was pre-heated at 105 °C for 20 min under magnetic stirring. Then, 1.0 mL of DEG containing Na₂PdCl₄ (15.5 mg) was rapidly injected into the vial with a pipette. The reaction was allowed to proceed at 105 °C for 24 h.

For the synthesis of Pd icosahedra 17 nm in size,^[16] 2.0 mL of EG containing PVP (30 mg) was placed in a 20 mL vial. The mixture was pre-heated at 160 °C for 20 min under magnetic

stirring. Meanwhile, H₂PdCl₄ was prepared by dissolving PdCl₂ in a mixture of EG and 37% (v/v) HCl, in which the molar ratio of HCl to PdCl₂ was set to 4/1 and the concentration of Pd(II) to 50 mM. Then, 1 mL of the H₂PdCl₄ solution (50 mM) was added into the vial in one shot. A specific amount of HCl was also added to achieve a final concentration of 134 mM in the reaction mixture. The reaction was allowed to proceed at 160 °C for 3 h.

All the syntheses were quenched by immersing the vials in an ice-water bath and the products were washed with acetone once and deionized (DI) water five times by centrifugation prior to the electrochemical measurements.

Characterization

The TEM images were taken using a microscope (HT7700, Hitachi) operated at 120 kV by drop-casting the nanoparticle dispersions on carbon-coated copper grids and drying under ambient conditions. The particle concentration of each suspension of Pd nanocrystals was determined using inductively coupled plasma mass spectrometry (ICP-MS, NexION 300Q, Perkin-Elmer).

Electrochemical measurements

Approximately 0.2 mg of the Pd nanocrystals and commercial Pd black (Strem Chemicals) were dispersed in 1.0 mL of DI water and treated by ultrasonic for 10 min. To prepare the working electrode, 10 µL of an aqueous suspension of the catalyst was dropped onto the precleaned glassy carbon electrode (Bioanalytical Systems Inc.). Upon drying in an oven at 50 °C for 10 min, the electrode was covered with 5 µl of Nafion aqueous solution (0.05%) and allowed to dry in an oven set to 50 °C for another 10 min. Then, plasma etching (PE-50, Plasma Etch Inc.) was carried out for 30 min to remove the PVP on the surfaces of the Pd catalysts. An Ag/AgCl electrode and a Pt mesh (1×1 cm²) were used as the reference and counter electrodes, respectively. The potentials are presented with a reference to RHE. To further remove the capping agents such as PVP, Br⁻, and I⁻, the electrical potential was held at -0.05 V for 60 s.^[7] CVs were obtained by cycling the potential between 0.08 and 0.8 V for 10 cycles in N₂-saturated 0.1 M HClO₄ solutions at a scan speed of 50 mV s⁻¹. The ECSAs were obtained from the charges associated with the stripping of Cuupp on the Pd nanocrystals by assuming 420 and 490 μ C cm⁻² for a full monolayer coverage of Cu on Pd enclosed by {100} and {111} facets, respectively, and 460 μ C cm⁻² for commercial Pd black.^[7] The Cu_{UPD} was conducted in a N2-saturated solution containing 0.05 M H2SO4 and 0.05 M CuSO4. To obtain

FAO activity, the catalyst was tested between 0.08 and 1.1 V for two cycles in a N₂-saturated solution containing 0.5 M HClO₄ and 0.5 M HCOOH at a scan speed of 50 mV s⁻¹. All the electrochemical measurements were conducted with a CHI600E potentiostat (CH Instrument).

Theoretical calculations

All calculations were performed using DACAPO. [31,32] A 3×3 unit cell was used to construct a four layer Pd(100) slab (36 slab atoms in total). A 1×3 unit cell was used to construct a ten layer Pd(211) slab (30 slab atoms in total). A 3×3 unit cell was used to construct a three layer Pd(111) slab (27 slab atoms in total). The surface coverage of adsorbates on all three surfaces was set to 1/9 ML, with only one adsorbate per unit cell. Each unit cell was repeated in super cell geometries with successive slabs separated by a vacuum region of at least 10 Å. The optimized bulk lattice constant for Pd was calculated to be 3.99 Å, in good agreement with the experimental value of 3.89 Å.[33] Adsorption was only allowed on one of the two exposed surfaces, with the electrostatic potential being adjusted accordingly. [34,35] The top two layers of the Pd(100) slab were relaxed and the top five layers of the Pd(211) slab were relaxed, whereas all layers of the Pd(111) slab were fixed since the effect of relaxation for this surface was negligible. [36] The surface Brillouin zone was sampled using a 4×4×1 Monkhorst-Pack kpoint mesh^[37] for Pd(211) and Pd(100), and was sampled using 18 special k-points^[38] for the Pd(111) surface. The Kohn-Sham one-electron valence states were expanded in a basis of plane waves with kinetic energies up to 25 Ry, and ionic cores were described by ultrasoft Vanderbilt pseudopotentials. [39] The exchange-correlation potential and energy were described self-consistently using the GGA-PW91 functional.[40,41] The electron density was determined by iterative diagonalization of the Kohn-Sham Hamiltonian, Fermi-population of the Kohn-Sham states ($k_BT = 0.1 \text{ eV}$), and Pulay mixing of the resulting electronic density. [42] The total energies were then extrapolated to $k_{\rm B}T=0$ eV. Convergence with respect to various calculation parameters was tested.

The binding energies (E_b) of the FAO intermediates were calculated with respect to the clean (relaxed, if applicable) surfaces ($E_{substrate}$) and the respective free adsorbate in the gas phase ($E_{gas-phase adsorbate}$), i.e., $E_b = E_{total} - E_{substrate} - E_{gas-phase adsorbate}$, where E_{total} is the energy of the surface with the adsorbate adsorbed on it. The surface intermediates being considered were COOH, HCOO, CO, and OH. Their E_b are presented in Table S1.

The thermochemistry of the elementary steps in the following reaction network was calculated using these E_b :

- 1. $HCOOH(g) + * \rightarrow HCOO^* + H^+ + e^-$
- 2. $HCOO^* \rightarrow CO_2(g) + H^+ + e^-$
- 3. $HCOOH(g) + * \rightarrow COOH^* + H^+ + e^-$
- 4. $COOH^* \rightarrow CO_2(g) + H^+ + e^-$
- 5. $COOH^* + * \rightarrow CO^* + OH^*$

The calculated reaction thermochemistry for proton/electron transfer reactions (elementary steps 1-5 above) were adjusted to an artificial electrode potential of 0.4 V using an approach similar to that of Nørskov and coworkers. [17,43-46] First, we chose the RHE as a reference. Under standard conditions, hydrogen gas is in equilibrium with protons and electrons, at a defined potential of 0 V. A change in the electrode potential by U will shift the free energy of each electron exothermically by eU, where e is the absolute charge of an electron. For this study, we have neglected the entropic and zero-point energy contributions to the free energy of the reactions because these corrections will not vary significantly between the surfaces.

Acknowledgements

This work was supported by startup funds from the Georgia Institute of Technology and by DOE-BES, Office of Chemical Sciences, grant DE-FG02-05ER15731. The computational work was performed in part using supercomputing resources from the following institutions: EMSL, a national scientific user facility at Pacific Northwest National Laboratory (PNNL); the Center for Nanoscale Materials at Argonne National Laboratory (ANL); and the National Energy Research Scientific Computing Center (NERSC). EMSL is sponsored by the Department of Energy's Office of Biological and Environmental Research located at PNNL. CNM and NERSC are supported by the U.S. Department of Energy, Office of Science, under contracts DE-AC02-06CH11357 and DE-AC02-05CH11231, respectively.

References

- [1] W. Vielstich, A. Lamm, H. A. Gasteiger in *Handbook of Fuel Cells Fundamentals, Technology and Applications*. John Wiley & Sons, Chichester, U.K., **2003**.
- [2] B. C. H. Steele, A. Heinzel, *Nature* **2001**, *414*, 345-352.
- [3] C. Rice, S. Ha, R. I. Masel, P. Waszczuk, A. Wieckowski, T. Barnard, *J. Power Sources* **2002**, *111*, 83-89.
- [4] A. Capon, R. Parsons, J. Electroanal. Chem. Interfacial Electrochem. 1973, 44, 1-7.

- [5] X. Yu, P. G. Pickup, J. Power Sources 2008, 182, 124-132.
- [6] Y.-W. Rhee, S. Y. Ha, R. I. Masel, J. Power Sources 2003, 117, 35-38.
- [7] M. Shao, J. Odell, M. Humbert, T. Yu, Y. Xia, J. Phys. Chem. C 2013, 117, 4172-4180.
- [8] H. Okamoto, W. Kon, Y. Mukouyama, J. Phys. Chem. B 2005, 109, 15659-15666.
- [9] A. Miki, S. Ye, M. Osawa, *Chem. Commun.* **2002**, 1500-1501.
- [10] N. Hoshi, K. Kida, M. Nakamura, M. Nakada, K. Osada, J. Phys. Chem. B 2006, 110, 12480-12484.
- [11] S. Ha, R. Larsen, R. I. Masel, J. Power Sources 2004, 144, 28-34.
- [12] Z. Niu, Q. Peng, M. Gong, H. Rong, Y. Li, Angew. Chem. Int. Ed. 2011, 50, 6315-6319.
- [13] X. Huang, S. Tang, X. Mu, Y. Dai, G. Chen, Z. Zhou, F. Ruan, Z. Yang, N. Zheng, Nat. Nanotechnol. 2011, 6, 28-32.
- [14] M. Jin, H. Zhang, Z. Xie, Y. Xia, Energy & Environ. Sci. 2012, 5, 6352-6357.
- [15] Y. Wang, S. Xie, J. Liu, J. Park, C. Z. Huang, Y. Xia, *Nano Lett.* **2013**, *13*, 2276-2281.
- [16] T. Lv, Y. Wang, S.-I. Choi, M. Chi, J. Tao, L. Pan, C. Z. Huang, Y. Zhu, Y. Xia, ChemSusChem 2013, 6, 1923-1930.
- [17] X. Xia, S.-I. Choi, J. A. Herron, N. Lu, J. Scaranto, H.-C. Peng, J. Wang, M. Mavrikakis, M. J. Kim, Y. Xia, J. Am. Chem. Soc. 2013, 135, 15706-15709.
- [18] Y. Xia, Y. Xiong, B. Lim, S. E. Skrabalak, Angew. Chem. Int. Ed. 2009, 48, 60-103.
- [19] H. Huang, Y. Wang, A. Ruditskiy, H.-C. Peng, X. Zhao, L. Zhang, J. Liu, Z. Ye, Y. Xia, ACS Nano 2014, 8, 7041-7050.
- [20] J. H. Conway, S. Torquato, Proc. Natl. Acad. Sci. U.S.A. 2006, 103, 10612-10617.
- [21] C. L. Johnson, E. Snoeck, M. Ezcurdia, B. Rodriguez-Gonzalez, I. Pastoriza-Santos, L. M. Liz-Marzan, M. J. Hytch, *Nat. Mater.* 2008, 7, 120-124.
- [22] M. R. Langille, J. Zhang, M. L. Personick, S. Li, C. A. Mirkin, *Science* 2012, 337, 954-957.
- [23] W. Zhou, J. Wu, H. Yang, Nano Lett. 2013, 13, 2870-2874.
- [24] R. Wang, H. Zhang, M. Farle, C. Kisielowski, *Nanoscale* **2009**, *1*, 276-279.
- [25] Y. Suo, I.-M. Hsing, *Electrochim. Acta* **2009**, *55*, 210-217.
- [26] H. C. Peng, S. Xie, J. Park, X. Xia, Y. Xia, J. Am. Chem. Soc. 2013, 135, 3780-3783.
- [27] A. Haji-Akbari, M. Engel, A. S. Keys, X. Zheng, R. G. Petschek, P. Palffy-Muhoray, S. C. Glotzer, *Nature* 2009, 462, 773-777.
- [28] A. Cuesta, L. A. Kibler, D. M. Kolb, J. Electroanal. Chem. 1999, 466, 165-168.
- [29] V. Viswanathan, H. A. Hansen, J. Rossmeisl, J. K. Nørskov, ACS Catalysis 2012, 2,

- 1654-1660.
- [30] J. Wu, L. Qi, H. You, A. Gross, J. Li, H. Yang, J. Am. Chem. Soc. 2012, 134, 11880-11883.
- [31] B. Hammer, L. B. Hansen, J. K. Nørskov, Phys. Rev. B 1999, 59, 7413-7421.
- [32] J. Greeley, J. K. Nørskov, M. Mavrikakis, Annu. Rev. Phys. Chem. 2002, 53, 319-348.
- [33] CRC Handbook of Chemistry and Physics. 92 ed.; CRC Press: New York, **2011**.
- [34] L. Bengtsson, Phys. Rev. B 1999, 59, 12301-12304.
- [35] J. Neugebauer, M. Scheffler, Phys. Rev. B 1992, 46, 16067-16080.
- [36] A. Kokalj, M. Causa, J. Phys.: Condens. Matter 1999, 11, 7463-7480.
- [37] H. J. Monkhorst, J. D. Pack, *Phys. Rev. B* **1976**, *13*, 5188-5192.
- [38] D. J. Chadi, M. L. Cohen, *Phys. Rev. B* **1973**, *8*, 5747-5753.
- [39] D. Vanderbilt, *Phys. Rev. B* **1990**, *41*, 7892-7895.
- [40] J. P. Perdew, J. A. Chevary, S. H. Vosko, K. A. Jackson, M. R. Pederson, D. J. Singh,C. Fiolhais, *Phys. Rev. B* 1992, 46, 6671-6687.
- [41] J. A. White, D. M. Bird, Phys. Rev. B 1994, 50, 4954-4957.
- [42] G. Kresse, J. Furthmuller, Comput. Mat. Sci. 1996, 6, 15-50.
- [43] J. K. Nørskov, J. Rossmeisl, A. Logadottir, L. Lindqvist, J. R. Kitchin, T. Bligaard, H. Jonsson, *J. Phys. Chem. B* **2004**, *108*, 17886-17892.
- [44] J. Rossmeisl, P. Ferrin, G. A. Tritsaris, A. U. Nilekar, S. Koh, S. E. Bae, S. R. Brankovic, P. Strasser, M. Mavrikakis, *Energy & Environ. Sci.* **2012**, *5*, 8335-8342.
- [45] P. Ferrin, A. U. Nilekar, J. Greeley, M. Mavrikakis, J. Rossmeisl, Surf. Sci. 2008, 602, 3424-3431.
- [46] A. U. Nilekar, M. Mavrikakis, Surf. Sci. 2008, 602, L89-L94.

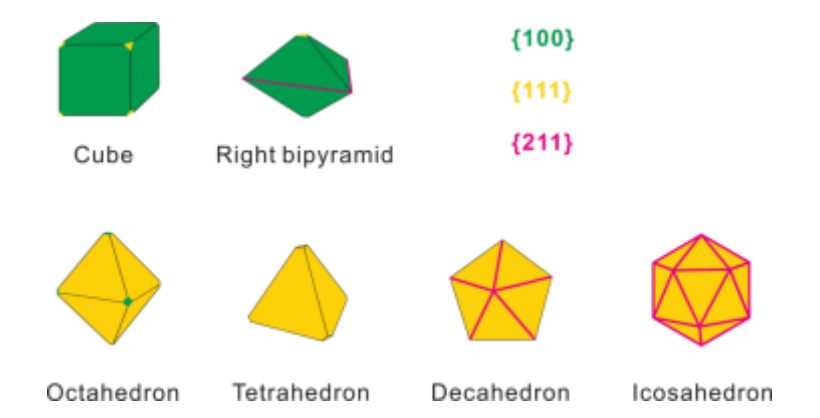
Table 1. Summary of the FAO activities of Pd nanocrystals with different shapes.

Shape of Pd nanocrystal	Size of nanocrystal (nm)	Number of twin boundaries	SA* at 0.4 V (mA cm ⁻²)	Anodic peak potential (V)	SA* at anodic peak potential (mA cm ⁻²)
Cube	15	-	5.9	0.54	10.1
Right bipyramid	15	1	9.1	0.56	20.8
Octahedron	13	-	5.0	0.47	6.0
Tetrahedron	15	-	3.0	0.40	3.0
Decahedron	15	5	7.4	0.47	10.0
Icosahedron	17	30	8.2	0.46	10.4

^{*}specific activity

Table 2. Relative stability of HCOO vs. COOH on model sites based on Pd(211), Pd(111), and Pd(100) surfaces. The energy of the more stable isomer on each surface is defined as the zero-energy reference for that surface. More positive entries signify less stable species. HCOO is practically isoenergetic with COOH on Pd(211) while COOH is more stable than HCOO on both Pd(111) and Pd(100).

Relative stability of isomers [eV]						
Adsorbate	Pd(211)	Pd(111)	Pd(100)			
HCOO	0.00	0.11	0.22			
СООН	0.01	0.00	0.00			



Scheme 1. Pd nanocrystals with different shapes, and the facets exposed on their faces, edges, and vertices.

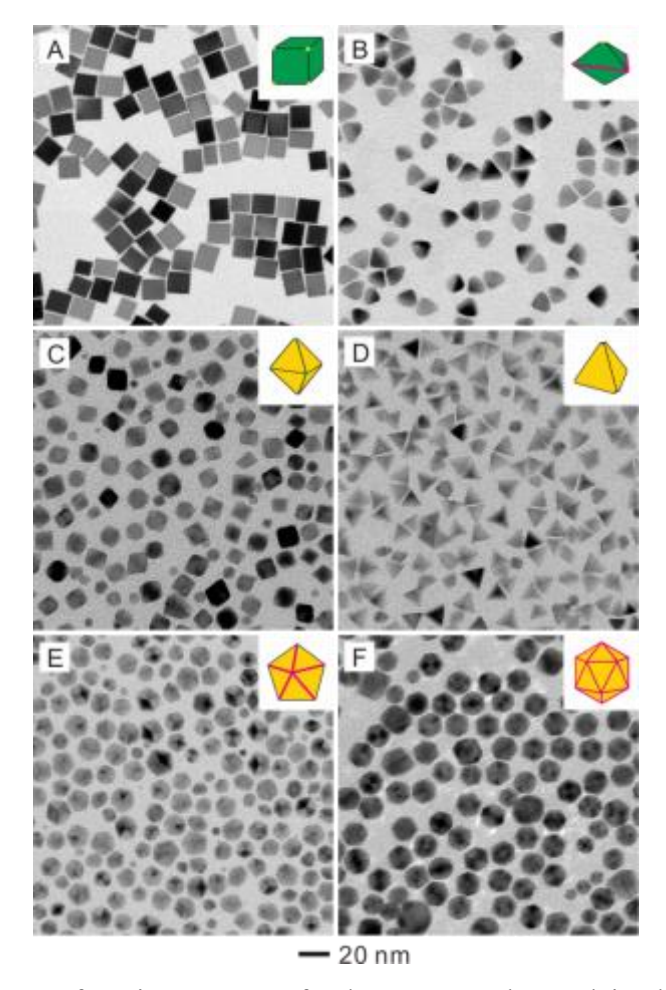


Figure 1. TEM images of various types of Pd nanocrystals used in the present study: (A) cubes, (B) right bipyramids, (C) octahedra, (D) tetrahedra, (E) decahedra, and (F) icosahedra. The nanocrystals had edge lengths of (A) 15, (B) 15, (C) 13, and (D) 15 nm, respectively. The diameters of Pd decahedra and icosahedra were 15 and 17 nm, respectively.

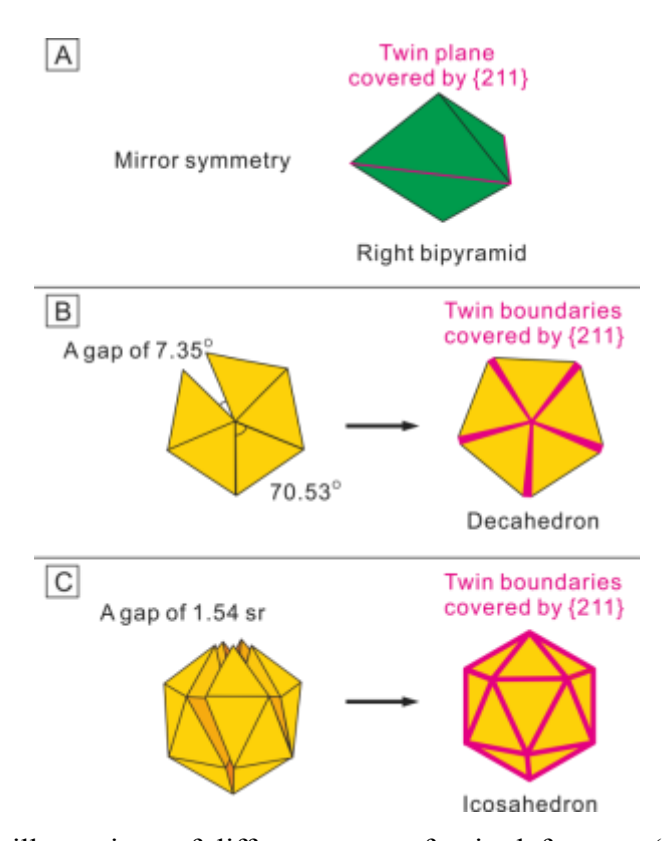


Figure 2. Schematic illustrations of different types of twin defects on (A) a right bipyramid, (B) a decahedron, and (C) an icosahedron. (A) The right bipyramid has a single twin defect, by which mirror symmetry is introduced into the crystal lattice. (B) The decahedron can be considered as an assembly of five single-crystal tetrahedra. There is a gap of 7.35° in the lattice as a result of the unique structure. (C) The icosahedron can be viewed as a densely packed array of twenty single-crystal tetrahedra. The icosahedron with a gap of 1.54 steradians (sr) will cause an internal lattice strain and a disordered region at the twin boundaries (similar to the twin zone of a decahedron).

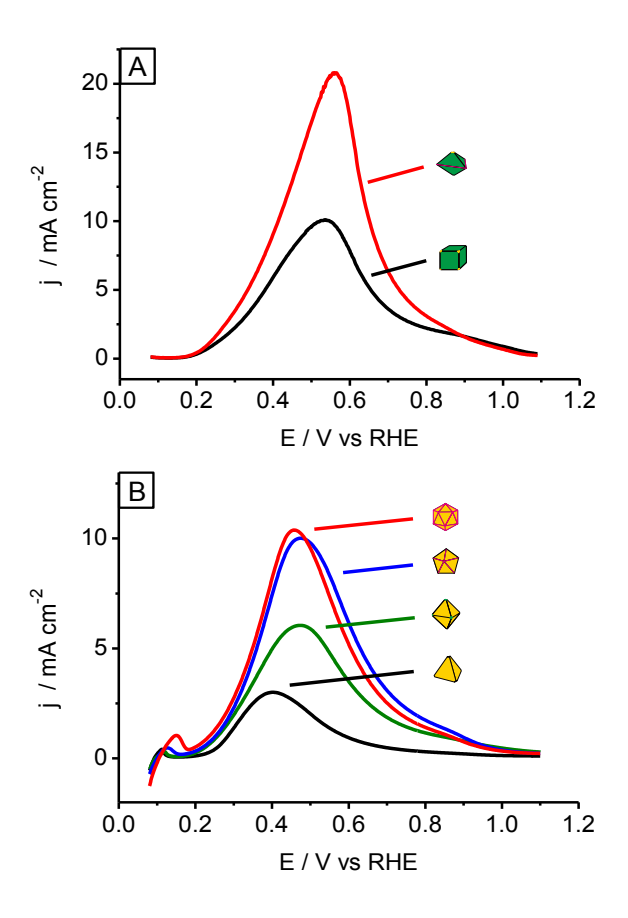


Figure 3. Anodic cyclic voltammograms for the FAO on Pd nanocrystals enclosed by (A) $\{100\}$ and (B) $\{111\}$ facets obtained in a N₂-saturated solution containing 0.5 M HClO₄ and 0.5 M HCOOH. Scanning speed = 50 mV s⁻¹. RHE = reversible hydrogen electrode. The currents were normalized to the electro-active surface areas of the corresponding Pd nanocrystals derived from the charges for the underpotential deposition of Cu. Schematic illustrations indicate the different shapes of Pd nanocrystals.

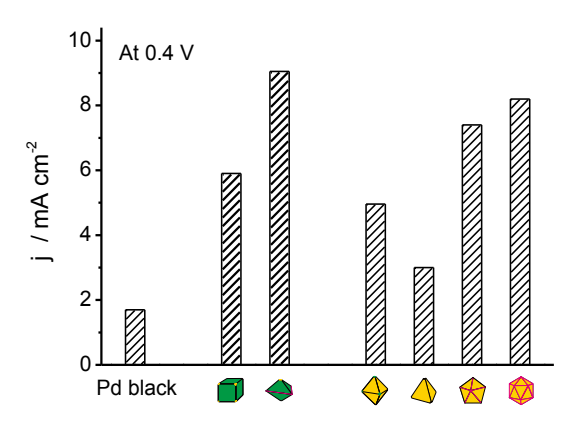


Figure 4. Comparison of the specific FAO activities on Pd nanocrystals with different shapes and twin structures at 0.4 V. The data were derived from Figure 3, A and B.

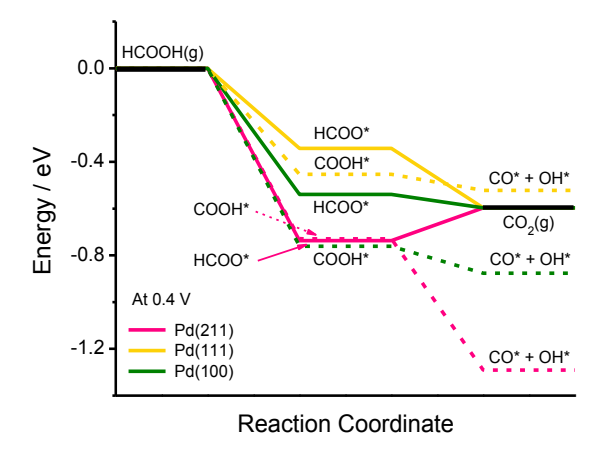


Figure 5. DFT-calculated thermochemical potential energy surfaces for the formic acid (HCOOH) oxidation at 0.4 V through HCOO-mediated (solid lines) and COOH-mediated (dashed lines) pathways on Pd(211) (magenta color), Pd(111) (yellow color), and Pd(100) (green color). The reaction stoichiometry is balanced with H^+ and e^- . For example, the energy level indicated by HCOO* corresponds to HCOO* $+ H^+ + e^-$.